2021 American Control Conference (ACC)
New Orleans, USA, May 25-28, 2021

Fast Charging-Minimum Degradation Optimal Control of Series-Connected Battery Modules with DC/DC Bypass Converters*

Vahid Azimi[1], Anirudh Allam[1], Won Tae Joe[2], Yohwan Choi[2], and Simona Onori[1], *Senior Member, IEEE*

***Abstract*— This paper presents a multi-objective fast charging-minimum degradation optimal control problem (OCP) for a Lithium-ion battery series-connected module with DC/DC bypass converters. Each cell in the module is modeled via coupled nonlinear electrochemical, thermal, and aging dynamics. Due to the multiscale temporal nature of the model, a surrogate model for the solvent diffusion aging dynamics is developed to mitigate prohibitive simulation time. The multi-objective OCP is formulated to find a trade-off policy between fast charging and degradation decay. For this purpose, the direct collocation approach is utilized to transcribe the OCP to a nonlinear programming (NLP) problem by parametrization of the system states, inputs, and charging times. The proposed OCP is formulated according to two different schemes: (i) same-charging-time (SCT) and (ii) different-charging-time (DCT). The former assumes simultaneous charging for all cells, whereas the latter determines different charging cell times. The performance of the proposed SCT and DCT schemes is validated on an illustrative case study of a battery module with two series-connected cells in the presence of initial state of charge imbalance.**

I. Introduction

Lithium-ion batteries (LIBs) have been extensively utilized in a wide range of applications including electrified vehicles, microgrids, consumer electronics, and smart grid energy storage [1], [2] thanks to their high cell voltage, high energy and power density, long battery life, and good cost performance [3]. Besides the standardly adopted constant-current constant-voltage (CCCV) charging protocol [4], strategies based on nonlinear programming (NLP) [5], single shooting [6], and model predictive control (MPC) [7] have been investigated to optimize charging of battery cells using electrochemical dynamics. On the other hand, to date, scant attention has been paid to battery pack/module charging.

A fundamental challenge when dealing with battery modules, as opposed to battery cells, is the intrinsic hetereogeneity among the cells in terms of thermal, and charge parameters such as state of charge (SOC) and depth of discharge (DOD) [8], [9]. This can lead to cell imbalance in the battery module, resulting in accelerated individual cell aging and nonuniform degradation across the cells. These challenges add complexity in the development of battery management system (BMS).

[1]Energy Resources Engineering Department, Stanford University, Stanford, CA 94305 USA (e-mail: vazimi@stanford.edu; aallam@stanford.edu; sonori@stanford.edu).

[2]LGES, e-Platform Developement Project Team, 36, Janggunmaeul 3-gil, Gwacheon-si, Gyeonggi-do, South Korea.

*The authors are grateful to LGES for its financial support, and helpful discussion and directions toward this project.

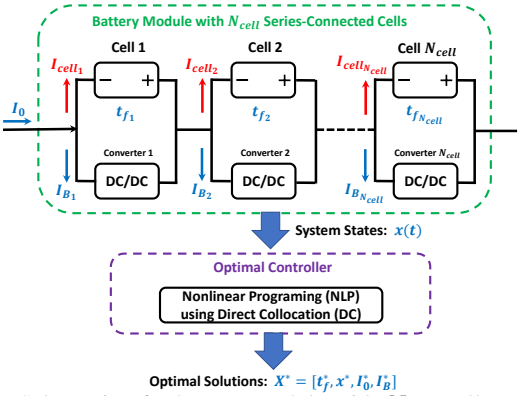

Fig. 1: Schematic of a battery module with N_{cell} cells connected in series, where each cell is connected in parallel to a DC-DC bypass converter. The variables annotated in blue are the variables to be optimized, where $\boldsymbol{I_B} = [I_{B_1}, \ldots, I_{B_{N_{cell}}}]^T$ and $\boldsymbol{t_f} = [t_{f_1}, \ldots, t_{f_{N_{cell}}}]^T$.

The majority of the work done at the pack/module level has been motivated by cell unbalance and geared towards the development of novel balancing approaches [10]–[12]. However, there is a current gap addressing optimal battery module charging. A charging strategy is one of the most crucial factors that can cause the battery degradation. Since charging and degradation are tightly coupled and are two conflicting objectives, simultaneous minimization of those is not possible. Hence, an optimal strategy is needed to charge the battery module as fast as possible while taking the degradation process into consideration. To the best of our knowledge, to date, no study has focused on a multi-objective fast charging and minimum degradation optimal control of battery modules with DC/DC bypass converters.

In this paper, the system under investigation is a LIB module with series-connected cells in which each cell is equipped with a DC/DC bypass converter (see Fig. 1). Each cell is described by coupled nonlinear partial differential equations (PDEs), ordinary differential equations (ODEs), and differential algebraic equations (DAEs) describing the electrochemical, thermal, and aging dynamics. The main contributions of this paper are fourfold: (i) Present a surrogate model of solvent diffusion dynamics to mitigate prohibitive simulation time of the multiscale temporal nature of the model; (ii) Design a multi-objective OCP for fast charging and minimum degradation of a battery module with N_{cell} series-connected cells shown in Fig. 1; (iii) Formulate the proposed strategy for two different schemes: (a) *same-charging-time* (SCT) and (b) *different-charging-time* (DCT), and propose an algorithm to solve them; and (iv) Demonstrate the validity of the proposed schemes on a case study of a battery module

with two series-connected cells.

First, we present a joint optimization/curve fitting approach to calculate solvent concentrations as functions of cell current and ambient temperature. This mitigates prohibitive simulation times due to the different time scales in the dynamics stemming from the solvent diffusion PDEs. With the high-fidelity battery module model in hand, a nonlinear OCP is formulated and solved to determine an optimal trade-off between fast charging and minimum degradation. For this purpose, the direct collocation (DC) approach [13] is utilized to transcribe the OCP to an NLP problem. We then employ the interior point solver IPOPT [14] to solve the NLP problem. Finally, to confirm the soundness of the proposed SCT and DCT schemes, simulation studies are carried out on an illustrative example: a battery module with two series-connected cells.

II. Battery Cell and Module Models

This section recalls the models for the LIB cell, and module with N_{cell} series-connected cells [15] in which each cell is modeled with coupled nonlinear PDEs, ODEs, and DAEs representing the electrochemical, thermal, and aging dynamics as presented in Table I. Throughout this section, the subscript i indicates the discretization grid position when converting the spatial directions of the solid electrodes and solid phase diffusion PDEs into ODEs. The subscript $j \in [n; p]$ refers to the cell domain (e.g. n = anode and p = cathode) and the superscript k represents the cell position within the module. Note that the main difference between the model presented in this paper and the one in [15] is that now each cell of the battery module is connected in parallel to a DC/DC converter.

Cell electrochemical model. We use the single particle model (SPM) to describe the electrochemical dynamics realized by the governing diffusion-like PDE in (1). The surface overpotentials η_j are calculated utilizing electrode surface and *constant* averaged electrolyte concentration for each domain (see (2)(a)), and the exchange current density is calculated for each electrode as in (2)(b). From the concentration and potential in each electrode, the cell voltage V_{cell} is calculated as in (3) in which the cell ohmic resistance includes the lumped contact R_l, electrolyte R_{el}, and SEI layer R_{sei} resistances. The cell voltage is also dependent on the open circuit potentials of each electrode U_j with $j \in [n, p]$ that are calculated using empirical relationships based upon electrode surface concentration stoichiometry. Further details about this model can be found in [16].

Cell thermal model. The cell thermal dynamics are modeled using a lumped parameter two-state thermal model, including core T_c and surface T_s temperatures as in (4).

Cell aging model. A physics-based approach is employed for battery aging that considers anode SEI layer growth as a function of solvent reduction kinetics and diffusion dynamics across the growing SEI layer in order to predict cell capacity loss and power fade. The solvent concentration available for reduction reaction at the anode surface is modeled by (5). The SEI layer growth (6)(a) has a linear relationship with side-reaction current (7) and the capacity loss is modeled by integrating side reaction current across the anode active surface area (see (6)(b)).

Discretization and model parameters. To solve the electrochemical and aging dynamics, PDEs with spatial dependence are discretized using Finite Difference Method (FDM). Solid electrode parameters, including $D_{s,j}$ and k_j, follow an Arrhenius relationship with temperature as reported in [17]. Empirical relationships for concentration and temperature dependencies of electrolyte parameter $k_{e,j}$ are adopted from [18].

State-space representation: cell-level. The governing PDEs are transformed into a system of ODEs and DAEs whose state-space description is given below.

Solid phase diffusion. The electrodes' state-space system is given by

$$\dot{\boldsymbol{c}}_{s,j} = \alpha_{s,j} A_{s,j} \boldsymbol{c}_{s,j} + \beta_{s,j} B_{s,j} \left[I_{cell} - g_{s,j} \right], \tag{8}$$

where $\boldsymbol{c}_{s,j} = [c_{s,j,1}, \ldots, c_{s,j,N_{r,j}}]^T \in \mathbb{R}^{N_{r,j}}$ with $c_{s,j,N_{r,j}} = c_{s,j}^{surf}$, $B_{s,j} = \left[0, \ldots, (2 + \frac{2}{N_r - 1})\right]^T \in \mathbb{R}^{N_{r,j}}$,

$$A_{s,j} = \begin{bmatrix} -2 & 2 & 0 & 0 & \ldots & 0 & 0 \\ 1/2 & -2 & 3/2 & 0 & \ldots & 0 & 0 \\ 0 & 2/3 & -2 & 4/3 & \ldots & 0 & 0 \\ \vdots & \vdots & \vdots & \vdots & \ddots & \vdots & \vdots \\ 0 & 0 & 0 & 0 & \ldots & 2 & -2 \end{bmatrix} \in \mathbb{R}^{N_{r,j} \times N_{r,j}}, \tag{9}$$

$$\alpha_{s,j} = \frac{D_{s,j}}{\Delta r_j^2},\ \beta_{s,j} = \begin{cases} \dfrac{-1}{AL_j F a_{s,j} \Delta r_j} & \text{if } j = n \\ \dfrac{1}{AL_j F a_{s,j} \Delta r_j} & \text{if } j = p \end{cases}, \tag{10}$$

and

$$g_{s,j}(c_{s,j}^{surf}, c_{solv}^{surf}, T_c, I_{cell}, L_{sei}) = \begin{cases} a_{s,n} L_n A i_s & \text{if } j = n \\ 0 & \text{if } j = p \end{cases} \tag{11}$$

with $\Delta r_j = \frac{R_{s,j}}{N_{r,j} - 1}$ and $N_{r,j}$ as the number of radial discretization grids in SPM for each electrode.

SEI layer growth. The state space of aging is given by

$$\dot{L}_{sei} = \beta_{sei} g_{s,n} \quad \text{with} \quad \beta_{sei} = \frac{-M_{sei}}{2F \rho_{sei} a_{s,n} L_n A}. \tag{12}$$

Solvent diffusion. The solvent diffusion state-space is presented as follows

$$\dot{\boldsymbol{c}}_{solv} = \begin{cases} 2\alpha_{solv}(c_{solv,2} - c_{solv,1}) + \\ \qquad \beta_{solv} \left(\dfrac{i_s}{F} - \dfrac{dL_{sei}}{dt} c_{solv,1} \right), & \text{if } i = 1 \\ \alpha_{solv} \left(c_{solv,i+1} - 2c_{solv,i} + c_{solv,i-1} \right) + \\ \qquad \gamma_{solv} \left(c_{solv,i+1} - c_{solv,i-1} \right), & \text{if } 1 < i < N_{sei} \\ 0, & \text{if } i = N_{sei} \end{cases} \tag{13}$$

$$\text{with} \quad \alpha_{solv} = \frac{D_{solv}}{(L_{sei} \Delta \xi)^2}, \quad \gamma_{solv} = \left(\frac{\xi - 1}{2 L_{sei} \Delta \xi} \frac{dL_{sei}}{dt} \right), \quad \beta_{solv} = \left(\frac{2}{L_{sei} \Delta \xi} + \frac{1}{D_{solv}} \frac{dL_{sei}}{dt} \right), \tag{14}$$

where $\boldsymbol{c}_{solv} = [c_{solv,1}, \ldots, c_{solv,N_{sei}}]^T \in \mathbb{R}^{N_{sei}}$ with $c_{solv,1} = c_{solv}^{surf}$; N_{sei} is the number of SEI layer discretization

TABLE I: Electrochemical-thermal-aging dynamics of an LIB cell.

Electrochemical dynamics: Mass conservation in solid phase	$\frac{\partial c_{s,j}}{\partial t} = \frac{D_{s,j}}{r^2}\frac{\partial}{\partial r}\left[r^2\frac{\partial c_{s,j}}{\partial r}\right], \quad j \in [n,p]$ $\frac{\partial c_{s,j}}{\partial r}\Big\|_{r=0} = 0 \quad \frac{\partial c_{s,j}}{\partial r}\Big\|_{r=R_{s,j}} = \frac{\pm I_{cell}}{D_{s,j}a_{s,j}AL_jF} + g_{s,j}(C_{s,j}^{surf}, C_{solv}^{surf}, T_c, I_{cell}, L_{sei})$	(1)
Electrode overpotential and exchange current density	(a) $\eta_j = \frac{R_gT_c}{0.5F}sinh^{-1}\left(\frac{I_{cell}}{2Aa_{s,j}L_ji_{0,j}}\right)$, (b) $i_{0,j} = k_j\sqrt{c_{e,j}^{avg}c_{s,j}^{surf}\left(c_{s,j}^{max} - c_{s,j}^{surf}\right)}, \quad j \in [n,p]$	(2)
Cell voltage	$V_{cell} = U_p(c_{s,p}^{surf}) + \eta_p(c_{s,p}^{surf}, c_{e,p}^{avg}, T_c, I_{cell}) - U_n(c_{s,n}^{surf}) - \eta_n(c_{s,n}^{surf}, c_{e,n}^{avg}, T_c, I_{cell}) - I_{cell}(R_l + R_{el} + R_{sei})$	(3)
Thermal dynamics: Cell core and surface heat balance	(a) $C_c\frac{dT_c}{dt} = I_{cell}(V_{oc} - V_{cell}) + \frac{T_s - T_c}{R_c}$, (b) $C_s\frac{dT_s}{dt} = \frac{T_{amb} - T_s}{R_u} - \frac{T_s - T_c}{R_c}$	(4)
Aging dynamics: Mass conservation in SEI	$\frac{\partial c_{solv}}{\partial t} = D_{solv}\frac{\partial^2 c_{solv}}{\partial r^2} - \frac{dL_{sei}}{dt}\frac{\partial c_{solv}}{\partial r}, \quad -D_{solv}\frac{\partial c_{solv}}{\partial r}\Big\|_{r=R_{s,n}} + \frac{dL_{sei}}{dt}c_{solv}^{surf} = \frac{i_s}{F}, \quad c_{solv}\Big\|_{r=R_n+L_{sei}} = \epsilon_{sei}c_{solv}^{bulk}$	(5)
SEI layer growth and cell capacity loss	(a) $\frac{dL_{sei}}{dt} = -\frac{i_sM_{sei}}{2F\rho_{sei}}$, (b) $\frac{dQ}{dt} = i_sAL_na_{s,n}$	(6)
Side reaction current density	$i_s = -2Fk_f(c_{s,n}^{surf})^2c_{solv}^{surf}\exp\left[\frac{-\beta F}{R_gT_c}(\Phi_{s,n} - R_{sei}I_{cell} - U_s)\right]$	(7)

points; and $\Delta\xi = \frac{1}{N_{sei}-1}$ and $\xi = \frac{r-R_{s,n}}{L_{sei}}$.

Surrogate model for solvent diffusion dynamics. The different time scales in the electrochemical, thermal, and SEI layer growth and solvent diffusion dynamics, cause prohibitive simulation times. In particular, the solvent diffusion PDEs (5) have been found to be the major bottle neck. To mitigate this issue, we propose a surrogate model that captures the solvent diffusion dynamics (13) based on a joint optimization/curve fitting approach. For this purpose, the following unconstrained optimization problem is formulated to find the optimal c_{solv}^* in such a way that the error between SEI layer thicknesses from the SPM with and without solvent diffusion PDEs, i.e., L_{sei}^a and $L_{sei}^*|_{c_{solv}^*}$, respectively, is minimized for different values of I_{cell} and T_{amb}:

$$c_{solv}^* = \min_{c_{solv}} \|L_{sei}^a - L_{sei}^*\|. \tag{15}$$

Once the optimal values c_{solv}^* are found for each current I_{cell} and ambient temperature T_{amb}, 5^{th}-other polynomials $G(I_{cell}, T_{amb})$ are fitted to the optimal points for all currents and each ambient temperature. The end result of this joint optimization/fitting approach is a surrogate model for the solvent diffusion from which the optimal solvent concentration can be computed for each T_{amb} as $c_{solv}^* = G_k(I_{cell}, T_{amb_k})$, where G_k is the function that calculates c_{solv}^* at the k^{th} ambient temperature. In this work, we consider I_{cell} to be discretely sampled within the range $[-6 \quad -0.5]$ A. Besides, the MATLAB built-in functions *fminsearch* and *polyfit* are employed to solve the optimization (15) and fit the polynomials $G_k(.,.)$, respectively.

State-space representation: module-level. With having access to state vectors, input variables, and state-space matrices for each cell, a convenient shorthand notation for module-level dynamics with N_{cell} series-connected cells can be presented as follows

$$\begin{aligned}
\dot{\boldsymbol{c}}_{s,j}^{mod} &= A_{s,j}^{mod}\boldsymbol{c}_{s,j}^{mod} + B_{s,j}^{mod}\boldsymbol{u} - G_{s,j}^{mod} \\
\dot{\boldsymbol{L}}_{sei}^{mod} &= G_{sei}^{mod} \\
\dot{\boldsymbol{T}}^{mod} &= A_{therm}^{mod}\boldsymbol{T}^{mod} + B_{therm}^{mod}\boldsymbol{u} + G_{therm}^{mod}T_{amb},
\end{aligned} \tag{16}$$

for which the module-level block diagonal coefficient matrices are defined in [15], and the state vectors and input variables for each cell are concatenated to obtain the module state vector

$$\boldsymbol{x}(t) = [\boldsymbol{c}_{s,j}^{mod}, \boldsymbol{T}^{mod}, \boldsymbol{L}_{sei}^{mod}, \boldsymbol{Q}^{mod}]^T. \tag{17}$$

Cell-to-cell heat transfer. Modeling the heat transfer between cells in the battery module is essential to understand the thermal and aging effects in the module [19]. The key attribute of the module-level model is that its thermal dynamics can provide the direct interconnection between adjacent cells in the battery module

$$\begin{aligned}
C_s\frac{dT_{s_k}}{dt} = &\frac{T_{amb} - T_{s_k}}{R_u} - \frac{T_{s_k} - T_{c_k}}{R_c} + \\
&\frac{T_{s_k} - T_{s_{k+1}}}{R_m} + \frac{T_{s_k} - T_{s_{k-1}}}{R_m}.
\end{aligned} \tag{18}$$

It should be noted that (18) modifies the conventional two-state thermal model governing equations (4) by incorporating the cell-to-cell heat transfer terms.

III. Optimal Control Problem Formulation

In this section, we formulate a multi-objective OCP for fast charging and minimum degradation of a battery module with N_{cell} series-connected cells demonstrated in Fig. 1. The cells may have initial SOC, temperature, and state of health (SOH) imbalances. SOH includes Q and R_{sei} that are dependent on L_{sei}; cells with different values of L_{sei} result in SOH imbalance within the battery module. Given these imbalances, we propose to solve the OCP for two different formulations SCT and DCT, where the former assumes that all cells are charged simultaneously, while the latter considers different times of charging for different cells.

In view of Fig. 1, $I_0 = I_{cell_i} + I_{B_i}$ for $i = 1, \ldots, N_{cell}$ from which one holds

$$\begin{aligned}
\boldsymbol{I_{cell}} &= [I_{cell_1}, \ldots, I_{cell_{N_{cell}}}]^T \\
&= [I_0 - I_{B_1}, \ldots, I_0 - I_{B_{N_{cell}}}]^T.
\end{aligned} \tag{19}$$

During charging, the module current $I_0 \in \Re$ and the vector of balancing currents $\boldsymbol{I_B} = [I_{B_1}, \ldots, I_{B_{N_{cell}}}]^T \in \Re^{N_{cell}}$ are unknown and must be optimally selected by solving the optimization problem; the number of degrees of freedom (DoF) is $N_{DoF} = N_{cell} + 1$. Each cell is connected in parallel

to a DC/DC bypass converter[1] whose current is determined by the proposed optimal controller.

In light of the above objective, the following OCP is formally defined

$$\boldsymbol{X}^* = \underset{\boldsymbol{X}\in\Re^{N_{opt}}}{\text{argmin}}\ \alpha\beta_1 h(\boldsymbol{t_f}) + (1-\alpha)\beta_2 \left(g_1(\boldsymbol{L_{sei}}) + g_2(\dot{\boldsymbol{L}}_{\boldsymbol{sei}})\right) \tag{20}$$

where the vector of optimization variables $\boldsymbol{X}$ is comprised of the vector of final times of charging $\boldsymbol{t_f} = [t_{f_1}, \ldots, t_{f_{N_{cell}}}]^T \in \Re^{N_{cell}}$ (under DCT scheme), the system state $\boldsymbol{x}(t) \in \Re^{N_s}$, the module current I_0, and the balancing current $\boldsymbol{I_B}$ such that

$$\boldsymbol{X} = [\boldsymbol{t_f}, \boldsymbol{x}(t), I_0(t), \boldsymbol{I_B}(t)]^T \in \Re^{N_{opt}}. \tag{21}$$

The number of optimization variables is $N_{opt} = N_s + 2N_{cell} + 1$, and the continuously differentiable functions g_1, g_2, and $h(t_f)$ are defined as

$$\begin{aligned} g_1(\boldsymbol{L_{sei}}) &= \frac{1}{N_{cell}} \sum_{i=1}^{N_{cell}} L_{sei_i}, \\ g_2(\dot{\boldsymbol{L}}_{\boldsymbol{sei}}) &= \frac{1}{N_{cell}} \sum_{i=1}^{N_{cell}} \dot{L}_{sei_i}, \\ h(\boldsymbol{t_f}) &= \frac{1}{N_{cell}} \sum_{i=1}^{N_{cell}} t_{f_i}. \end{aligned} \tag{22}$$

Note that $g_1(\boldsymbol{L_{sei}}), g_2(\dot{\boldsymbol{L}}_{\boldsymbol{sei}})$, and $h(\boldsymbol{t_f})$ are operators that return the average of SEI layer thicknesses, the average of their rates, and the average of charging times, respectively. Thus, the OCP (20) along with the definitions (22) forms a *min-mean optimization problem*. Besides, $\beta_1, \beta_2 > 0$ are the optimization weights and $0 \leq \alpha \leq 1$ is a trade-off coefficient that can be adjusted for three different paradigms: fast charging ($\alpha = 1$), minimum degradation ($\alpha = 0$), and balanced charging-degradation ($0 < \alpha < 1$). The operation of the battery module is subject to the dynamic constraints (16) and the following *task constraints*

$$\begin{aligned} &I_{B_{\min}} \leq I_{B_i}(t) \leq I_{B_{\max}}, \quad I_{0_{\min}} \leq I_0(t) \leq I_{0_{\max}}, \\ &SOC_i(t_f) = SOC_{\text{target}}, \quad SOC_i(t_0) = SOC_{\text{initial}_i}, \\ &V_{cell_i}(t) \leq V_{cell\max}, \quad 0 \leq t_{f_i} \leq t_{f_{\max}}, \\ &L_{sei_i}(t_0) = L_{sei_{0_i}}, \quad Q_i(t_0) = Q_{0_i}, \\ &T_{ji}(t_0) = T_{ji_0}, \quad T_{ji_{\min}} \leq T_{ji}(t) \leq T_{ji_{\max}}, \quad j \in \{c, s\}, \\ &\theta^j_{0\%} c^{\max}_{s,j} \leq c_{s_j}(t) \leq \theta^j_{100\%} c^{\max}_{s,j}, \quad j \in \{n, p\}, \end{aligned} \tag{23}$$

where $i = 1, \ldots, N_{cell}$. It should be pointed out that for a given N_r, the number of states is calculated as $N_s = N_{cell}\,(4 + 2(N_r - 1))$.

Despite the cell imbalance in the battery module, one might consider the simultaneous charging of the cells; this can be realized through the SCT formulation. To implement SCT, the OCP resembles the DCT scheme except for the following discrepancies.

(a) The final times of charging are the same for all cells, which implies that $t_f \in \Re$.
(b) The number of optimization variables is $N_{opt} = N_s + N_{cell} + 2$.
(c) The cost function associated with charging reduces to $h(t_f) = t_f$.
(d) The constraint associated with the charging time reduces to $0 \leq t_f \leq t_{f_{\max}}$.

Since the dynamic constraints (16) are nonlinear and coupled, the problem (20) subject to (16) and (23) can be solved using a nonlinear optimization problem. In this paper, we utilize the DC approach [13] to transcribe the original OCP (20) to an NLP problem by approximating all elements of the unknown vector $\boldsymbol{X}$ as polynomial splines. Spline approximates a continuous trajectory by combining a sequence of polynomial segments that are glued together at given break points (BPs). This way all trajectories are discretized in time $0 = t_0 < t_1 < \cdots < t_{N_{BP}} = t_f$, where N_{BP} is the number of BPs, and t_0 and t_f are the initial and final times, respectively.

By approximating all of the system trajectories $\boldsymbol{t_f}$, $\boldsymbol{x}(t)$, $I_0(t)$, and $\boldsymbol{I_B}(t)$, the original OCP (20) can be transcribed to the NLP problem using the DC approach under which the cost and constraints are applied to the optimization variables at collocation points (CPs) which differ from the BPs. After transcription of the OCP to the NLP problem using the DC, the well-developed interior point solver IPOPT [14] can be employed to solve the NLP problem. All dynamic and task constraints, and the cost are written symbolically by making use of the Matlab symbolic toolbox. This formulation provides symbolic differentiation of the OCP, which in turn, results in remarkable improvement in convergence time and solving reliability.

IV. Simulation Results

In this section, we validate the effectiveness of the proposed optimal control algorithm for both SCT and DCT formulations on a battery module with two series connected cells (i.e., $N_{cell} = 2$), where for each cell, a DC/DC bypass converter is connected in parallel (see Fig. 1). Throughout the simulations, we assume that there is an initial SOC imbalance among the cells ($SOC_1(0) \neq SOC_2(0)$), while no mismatch between temperatures, SEI layer thicknesses, and capacities of individual battery cells is assumed. The physical bounds in (23) are set to $I_{B_{\min}} = I_{0_{\min}} = -6\ A$, $I_{B_{\max}} = 0\ A$, $I_{0_{\max}} = -0.5\ A$, $SOC_i(t_f) = 0.8$, $V_{cell\max} = 4.2\ V$, $t_{f_{\max}} = 2000\ s$, $T_{ji_{\min}} = 5°C$, and $T_{ji_{\max}} = 45°C$ with $j \in \{c, s\}$ and $i = 1, 2$. The initial conditions are picked as $L_{sei_i}(0) = 5 \times 10^{-9}\ m$, $Q_i(0) = 2\ Ah$, and $T_{ci}(0) = T_{si}(0) = T_{amb}$ (i.e., starting from the rest). To provide the *balanced charging-degradation protocol*, the optimization weights and the trade-off coefficient are adjusted to be $\beta_1 = 1$, $\beta_2 = 5 \times 10^8$, and $\alpha = 0.5$.

It can be seen from Fig. 2 that despite the initial SOC mismatch, both cells are charged simultaneously at $t_f = 985\ s$ (with different rates) while the cell voltages are bounded by $V_{cell\max} = 4.2\ V$. As observed in this figure, in contrast with Cell 2, Cell 1 that has lower initial SOC ages more, loses more capacity, obtains higher final core and surface temperatures,

[1]The temperature effects on the DC/DC bypass converters will be the subject of future investigation.

TABLE II: Performance comparison between the SCT and DCT formulations with initial SOC mismatch $SOC_1(0) = 0.2$ and $SOC_2(0) = 0.4$ at $T_{amb} = 25°C$, where $\Delta z_i = \frac{|z_i(t_f) - z_i(t_0)|}{z_i(t_0)} \times 100\%$ with $z \in \{L_{sei}, Q\}$ and $i = 1, 2$ denotes an operator that returns the variation of variable z_i with respect to its initial condition $z_i(t_0)$. The best value of each metric is shown in bold.

Scheme	$(\Delta L_{sei_1}, \Delta L_{sei_2})\%$	$(\Delta Q_1, \Delta Q_2)\%$	(t_{f_1}, t_{f_2}) s
SCT	(**8.240**, **7.364**)	(**0.021**, **0.018**)	(**985**, 985)
DCT	(9.920, 8.859)	(0.025, 0.022)	(1119, **807**)

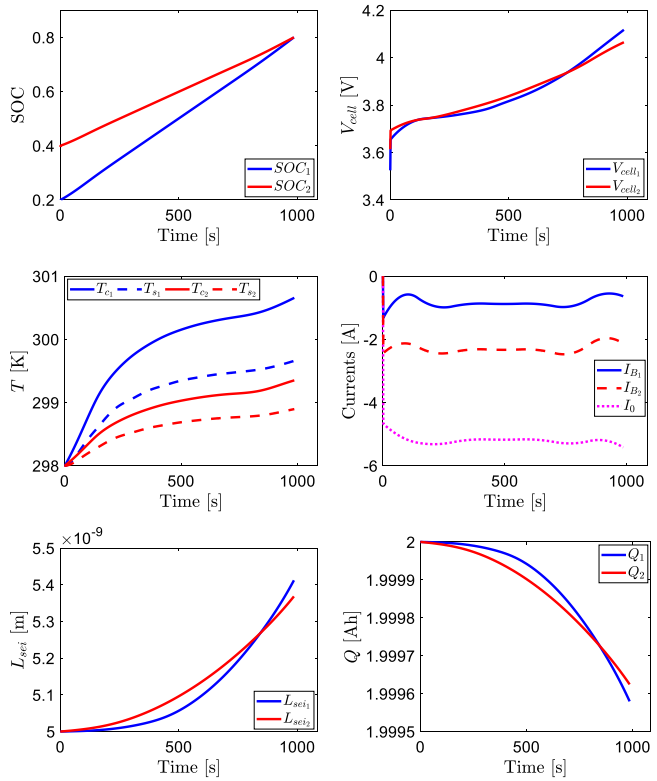

Fig. 2: Results from the multi-objective OCP for SCT formulation with initial SOC mismatch $SOC(0) = [0.2, 0.4]$ at $T_{amb} = 25°C$.

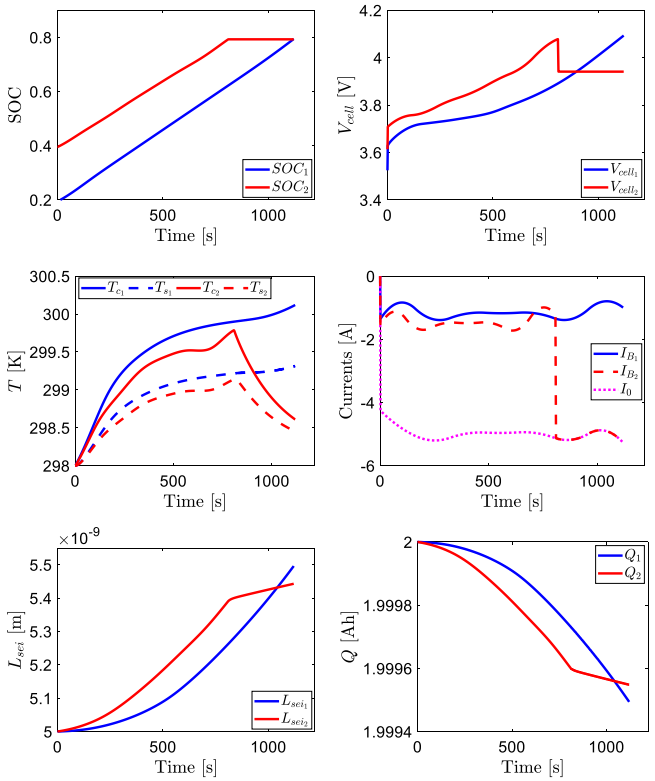

Fig. 3: Results from the multi-objective OCP for DCT formulation with initial SOC mismatch $SOC(0) = [0.2, 0.4]$ at $T_{amb} = 25°C$.

and absorbs greater current (the lower I_{B_1} results in the higher I_{cell_1}).

In contrast to SCT scheme under which simultaneous charging is achieved, charging times are different for different cells with the DCT scheme (see Fig. 3). As expected, the cell with higher initial SOC (i.e., Cell 2) is charged faster (at $t_{f_2} = 807\ s$) and then its SOC remains constant until the other cell (i.e., Cell 1) reaches the target SOC at $t_{f_1} = 1119\ s$ (the rates of charge are the same for different cells). As observed, once Cell 2 is charged, the whole current is absorbed by its DC/DC bypass converter which results in $I_0 = I_{B_2}$ over $t_{f_2} \leq t \leq t_{f_1}$. This, in turn, follows that (i) V_{cell_2} drops at t_{f_2} and remains constant afterwards, (ii) T_{c_2} and T_{s_2} start decreasing at t_{f_2}, and (iii) the rates of aging and capacity loss slow down for Cell 2 at $t = t_{f_2}$. Furthermore, Fig. 3 shows that the results obtained by DCT are consistent with ones from SCT scheme from which Cell 2 (the cell with higher initial SOC) ages less, loses less capacity, and meets lower final core and surface temperatures.

To compare the results of SCT and DCT, Table II lists quantitative comparisons between two schemes. According to this table, although DCT scheme charges the cell with higher initial SOC faster, the optimization under SCT scheme renders lower variations for L_{sei_i} and Q_i.

V. Discussion and Conclusion

This paper formulated a multi-objective fast charging-minimum degradation OCP for battery modules with N_{cell} series-connected cells with DC/DC bypass converters. Electrochemical-thermal-aging model of the battery module was provided. We introduced a joint optimization/curve fitting method to calculate the solvent concentrations as a remedy for prohibitive simulation times causing by the solvent diffusion dynamics. An OCP was developed with SCT and DCT schemes. DC approach was employed to transcribe the OCP to an NLP that was solved by IPOPT. To validate the effectiveness of SCT and DCT schemes, simulation studies were carried out on a battery module with two series-connected cells in the presence of initial SOC imbalance. Results for $SOC(0) = [0.2, 0.4]$ and $T_{amb} = 25°C$ showed that under both schemes, the cell with lower initial SOC ages more, loses more capacity, and obtains higher final core and surface temperatures. Finally, our findings showed that the

Nomenclature

$c_{s,j}$	Concentration in solid phase [mol/m^3]	$k_{e,j}$	Electrolyte conductivity [S/m]	c_{solv}	Solvent concentration [mol/m^3]
T_c	Cell core temperature [K]	T_s	Cell surface temperature [K]	L_{sei}	SEI layer thickness [m]
Q	Cell capacity [Ah]	I_{cell}	Cell current [A]	η_j	Overpotential [V]
$i_{0,j}$	Exchange current density [A/m^2]	U_j	Open circuit potential (electrode) [V]	V_{oc}	Open circuit potential (cell) [V]
i_s	Side reaction current density [A/m^2]	$D_{s,j}$	Solid phase diffusion [m^2/s]	$R_{s,j}$	Particle radius [m]
$a_{s,j}$	Specific interfacial surface area [m^{-1}]	A	Cell cross sectional area [m^2]	L_j	Domain thickness [m]
F	Faraday's constant [C/mol]	$c_{s,j}^{max}$	Maximum electrode concentration [mol/m^3]	R_m	Cell-to-cell heat transfer resistance [K/W]
k_j	Intercalation rate constant [m$^{2.5}$/s-mol$^{0.5}$]	R_l	Lumped contact resistance [Ω]	R_{el}	Electrolyte resistance [Ω]
R_{sei}	SEI layer resistance [Ω]	R_g	Universal gas constant [J/mol-K]	D_{solv}	Solvent diffusion coefficient in SEI layer [m^2/s]
ϵ_{sei}	SEI Layer porosity [-]	ρ_{sei}	SEI layer density [kg/m^3]	I_0, I_B	Module and balancing currents [A]
U_s	Solvent reduction potential [V]	M_{sei}	Molar mass of SEI layer [kg/mol]	$\Phi_{s,j}$	Surface potential [V]
C_s	Heat capacity of cell surface [J/K]	C_c	Heat capacity of cell core [J/K]	R_c	Conductive resistance - core/surface [K/W]
R_u	Convective resistance - surface/surroundings [K/W]	T_{amb}	Ambient temperature [K]	$N_{r,j}$	Number of radial discretization points [-]
N_{sei}	Number of SEI layer discretization points [-]	$c_{s,j}^{surf}$	Surface concentration in solid phase [mol/m^3]	c_{solv}^{surf}	Surface solvent concentration [mol/m^3]
$c_{e,j}^{avg}$	Average electrolyte concentration [mol/m^3]	N_s, N_{cell}	Number of states and cells [-]	α	Trade-off coefficient [-]
u	Cells' current [A]	$\theta_{0\%}^j$	Reference stoichiometry ratio at 0% SOC [-]	$\theta_{100\%}^j$	Reference stoichiometry ratio at 100% SOC [-]
k_f	Solvent reduction rate constant [mol^{-2}s^{-1}]	N_{BP}	Number of BPs [-]	c_{solv}^*	Optimal solvent concentration [mol/m^3]

optimization under SCT scheme renders lower variations of SEI layer thickness and capacity over the DCT formulation.

REFERENCES

[1] A. Hoke, A. Brissette, D. Maksimović, A. Pratt, and K. Smith, "Electric vehicle charge optimization including effects of lithium-ion battery degradation," in *2011 IEEE Vehicle Power and Propulsion Conference*, pp. 1–8, Sep. 2011.

[2] Y. Du, J. Wu, S. Li, C. Long, and S. Onori, "Hierarchical coordination of two-time scale microgrids with supply-demand imbalance," *IEEE Transactions on Smart Grid*, vol. 11, pp. 3726–3736, Sep. 2020.

[3] S. M. Lukic, J. Cao, R. C. Bansal, F. Rodriguez, and A. Emadi, "Energy storage systems for automotive applications," *IEEE Transactions on Industrial Electronics*, vol. 55, pp. 2258–2267, June 2008.

[4] K. Liu, K. Li, Z. Yang, C. Zhang, and J. Deng, "An advanced lithium-ion battery optimal charging strategy based on a coupled thermoelectric model," *Electrochimica Acta*, vol. 225, pp. 330 – 344, 2017.

[5] B. Suthar, P. W. C. Northrop, R. D. Braatz, and V. R. Subramanian, "Optimal charging profiles with minimal intercalation-induced stresses for lithium-ion batteries using reformulated pseudo 2-dimensional models," *Journal of The Electrochemical Society*, vol. 161, no. 11, pp. F3144–F3155, 2014.

[6] F. Lam, A. Allam, W. T. Joe, Y. Choi, and S. Onori, "Offline multiobjective optimization for fast charging and reduced degradation in lithium-ion battery cells using electrochemical dynamics," *IEEE Control Systems Letters*, pp. 1–1, 2020.

[7] C. Zou, C. Manzie, and D. Nešić, "Model predictive control for lithium-ion battery optimal charging," *IEEE/ASME Transactions on Mechatronics*, vol. 23, pp. 947–957, April 2018.

[8] A. Barré, B. Deguilhem, S. Grolleau, M. Gérard, F. Suard, and D. Riu, "A review on lithium-ion battery ageing mechanisms and estimations for automotive applications," *Journal of Power Sources*, vol. 241, pp. 680 – 689, 2013.

[9] F. Todeschini, S. Onori, and G. Rizzoni, "An experimentally validated capacitydegradation model for li-ion batteries inphevs applications," in *8th IFAC Symposium on Fault Detection,Supervision and Safety of Technical Processes*, vol. 45, pp. 456–461, 2012.

[10] F. Altaf, B. Egardt, and L. Johannesson Mårdh, "Load management of modular battery using model predictive control: Thermal and state-of-charge balancing," *IEEE Transactions on Control Systems Technology*, vol. 25, pp. 47–62, Jan 2017.

[11] M. Evzelman, M. M. Ur Rehman, K. Hathaway, R. Zane, D. Costinett, and D. Maksimovic, "Active balancing system for electric vehicles with incorporated low-voltage bus," *IEEE Transactions on Power Electronics*, vol. 31, pp. 7887–7895, Nov 2016.

[12] D. J. Docimo and H. K. Fathy, "Multivariable state feedback control as a foundation for lithium-ion battery pack charge and capacity balancing," *Journal of The Electrochemical Society*, vol. 164, pp. A61–A70, dec 2016.

[13] C. R. Hargraves and S. W. Paris, "Direct trajectory optimization using nonlinear programming and collocation," *AIAA J. Guidance*, vol. 10, no. 4, p. 338–342, 1987.

[14] A. Wachter, L. Biegler, Y. Lang, and A. Raghunathan, "Ipopt: An interior point algorithm for large-scale nonlinear optimization," *Advances in the Astronautical Sciences*, 2002.

[15] T. Weaver, A. Allam, and S. Onori, "A novel lithium-ion battery pack modeling framework - series-connected case study," in *2020 American Control Conference (ACC)*, pp. 365–372, July 2020.

[16] A. Allam and S. Onori, "An interconnected observer for concurrent estimation of bulk and surface concentration in the cathode and anode of a lithium-ion battery," *IEEE Transactions on Industrial Electronics*, vol. 65, no. 9, pp. 7311–7321, 2018.

[17] T. R. Tanim, C. D. Rahn, and C.-Y. Wang, "A Temperature Dependent, Single Particle, Lithium Ion Cell Model Including Electrolyte Diffusion," *Journal of Dynamic Systems, Measurement, and Control*, vol. 137, 08 2014.

[18] L. Valoen and J. Reimers, "Transport properties of lipf6-based li-ion battery electrolytes," *J. of The Electrochemical Society*, 2005.

[19] A. Allam, S. Onori, S. Marelli, and C. Taborelli, "Battery health management system for automotive applications: a retroactivity-based aging propagation study," in *American Control Conference (ACC), 2015*, pp. 703–716, IEEE, 2015.